

## Molecular Modeling Studies of $\beta$ -Sitosterol Extract from *Miconia burchellii* Triana (Melastomataceae) from Brazilian Cerrado

Marianna C. Silva,<sup>1b</sup>\*<sup>a</sup> Vitor S. Duarte,<sup>b</sup> Lôide O. Sallum,<sup>1b</sup><sup>a</sup> Gracielle O. S. Cunha,<sup>b</sup> Jean M. F. Custodio,<sup>c</sup> Allen G. Oliver,<sup>c</sup> Josana C. Peixoto,<sup>a,b</sup> Antônio C. S. Menezes<sup>b</sup> and Hamilton B. Napolitano<sup>1b</sup>\*<sup>a,b</sup>

<sup>a</sup>Laboratório de Novos Materiais, Universidade Evangélica de Goiás, 75083-515 Anápolis-GO, Brazil

<sup>b</sup>Grupo de Química Teórica e Estrutural de Anápolis, Universidade Estadual de Goiás, 75132-903 Anápolis-GO, Brazil

<sup>c</sup>Department of Chemistry and Biochemistry, University of Notre Dame, 46556 Notre Dame, IN, USA

The Brazilian Cerrado biome is considered one of the 25 hotspots worldwide that contain bioactive compounds due to its great biodiversity; however, the reduction of its native area over time due to the expansion of urbanization and agribusiness may have compromised knowledge of its biological variety. In this context, knowledge about Cerrado species can contribute to its biodiversity preservation. This study aims to describe the isolation, molecular architecture and theoretical calculations of the compound (3*S*,8*S*,9*S*,10*R*,13*R*,14*S*,17*R*)-17-[(2*R*,5*R*)-5-ethyl-6-methylheptan-2-yl]-10,13 dimethyl 2,3,4,7,8,9,11,12,14,15,16,17-dodecahydro-1*H*-cyclopenta[*a*]phenanthren-3-ol, extracted from the Brazilian Cerrado *Miconia burchellii* plant. The supramolecular arrangement was described by Hirshfeld surface analysis, demonstrating the intermolecular interactions in the crystalline packing. The structure-property relationship shows the electrostatic potential map analysis, which reveals that the oxygen region is susceptible to electrophilic attack, and the frontier molecular orbital confirmed the kinetic stability of this compound. This study represents another step forward in the knowledge of compounds with pharmacological and medicinal properties extracted from the Cerrado.

**Keywords:** Brazilian Cerrado, Melastomataceae,  $\beta$ -sitosterol, X-ray diffraction

### Introduction

The Brazilian Cerrado covers more than 200 million hectares in the central region of the country, and it is the second-largest biome in South America.<sup>1-3</sup> It is a highly heterogeneous landscape, and parts of it are severely threatened. Among those parts that need particular attention, the Cerrado-Amazon transition zone stands out, considering it has undergone heavy deforestation and presents highly unusual rupestrian fields.<sup>4,5</sup> The unique characteristics of the biome, such as long periods of drought, as well as its relief, altitude, and soil characteristics, have led to its varied phytophysiology.<sup>6,7</sup> The evaluation of the therapeutic potential of plant species from Cerrado's region and some of their constituents has been the subject of studies that result in the discovery of molecules with great potential for future

use as medicinal agents.<sup>8,9</sup> However, its native vegetation has decreased considerably due to urbanization and agribusiness, thus resulting in a lack of biological and medicinal knowledge of the Cerrado.<sup>10</sup> The *Miconia* genus is an example of under-researched vegetation and represents about 2% of the studied species.<sup>11</sup> Among the few studies carried out, 79 compounds belonging to different classes have been identified, with sterols representing 6% of this distribution.<sup>11</sup> The isolation and characterization of sterols from Cerrado plants are not restricted to the genus *Miconia* but also occur in *Caryocar*,<sup>12</sup> *Genipa*,<sup>13</sup> *Qualea*,<sup>14</sup> *Sebastiania*,<sup>3</sup> *Jatropha*,<sup>3</sup> *Poincianella*,<sup>3</sup> *Plathymenia*,<sup>15</sup> *Cecropia*,<sup>16</sup> *Myracrodruon*,<sup>16</sup> *Siparuna*,<sup>16</sup> *Strphnodedron*,<sup>16</sup> among others.

Phytosterols are isoprenoids that are part of the triterpene family, and their basic structure consists of 1,2-cyclopentane-phenanthrene-a hydroxyl group on the ring A, and an alkyl chain on C17.<sup>17</sup> The phytosterol structures vary in carbon side chains and saturation of the steroidal ring; for example,  $\beta$ -sitosterol differs from the basic structure due to the

\*e-mail: silva.c.marianna@gmail.com; hbnapolitano@gmail.com  
Editor handled this article: José Walkimar M. Carneiro

inclusion of an extra ethyl and isopropyl group in the side chain.<sup>18,19</sup> Sterols are abundantly found in the plant kingdom in fruits, nuts, cereals, and vegetables,<sup>11,20,21</sup> and their daily consumption is important as part of the diet.<sup>18</sup>  $\beta$ -Sitosterol is the most common phytosterol for the dietary treatment of hypercholesterolemia, contributing to the reduction of low-density lipoprotein cholesterol (LDL-C) in serum.<sup>18,22</sup> In addition, this compound has several biological activities, such as analgesic,<sup>23</sup> antimicrobial,<sup>24,25</sup> anti-cancer,<sup>26-28</sup> anti-inflammatory,<sup>23,29</sup> anti-fibrotic,<sup>30</sup> hepatoprotective,<sup>31</sup> antioxidant,<sup>32,33</sup> anti-diabetic.<sup>21,32,34,35</sup>

Based on the potential biological activities of sterol, and the need for knowledge of compounds extracted from native Cerrado plants, we present the isolation, crystallization, and identification of the compound (3*S*,8*S*,9*S*,10*R*,13*R*,14*S*,17*R*)-17-[(2*R*,5*R*)-5-ethyl-6-methylheptan-2-yl]-10,13-dimethyl 2,3,4,7,8,9,11,12,14,15,16,17-dodecahydro-1*H*-cyclopenta[*a*]phenanthren-3-ol (STR), extracted from the plant *Miconia burchellii*. The molecular and supramolecular architectures were characterized using single-crystal X-ray diffraction (XRD) and Hirshfeld surface (HS) analysis. To go deeper into the molecular structure studies, theoretical calculations such as frontier molecular orbitals (FMO) and the molecular electrostatic potential map (MEP) were carried out at the M06-2X/6-311++G(d,p) level of theory.

## Experimental

### Material

Solvents were purchased from the companies Neon (Suzano, Brazil), Anidrol (Diadema, Brazil), and Dinâmica (Indaiatuba, Brazil) and used without further purification. Thin layer chromatography (TLC) was performed on silica-gel F<sub>254</sub> Macherey-Nagel plates (Düren, Germany). Nuclear magnetic resonance (NMR) analyses were performed in 11.75 T Bruker equipment (500 MHz), Avance III model (Karlsruhe, Germany). The <sup>1</sup>H and <sup>13</sup>C chemical shifts were acquired with CDCl<sub>3</sub> as deuterated solvent and tetramethylsilane (TMS) as internal standard (Cambridge Isotope Laboratories, Tewksbury, USA). Chemical shifts ( $\delta$ ) are reported in parts per million (ppm). Infrared (IR) spectra were recorded on a PerkinElmer FTIR Frontier spectrometer (Waltham, USA) using KBr disc, and frequencies are expressed in cm<sup>-1</sup>.

### Plant material

The leaves from *Miconia burchellii* Triana (Melastomataceae) were collected in June 2018 at Serra dos

Pirineus, Goiás State, Brazil, at three different geographical coordinates (15°47'3" S, 48°48'37" W; 15°47'57" S, 48°49'10" W, and 15°47'52" S, 48°49'53" W). A voucher's specimens (No. 13931, 13932, and 13933) were deposited in the Herbarium of the State University of Goiás. Access to the genetic heritage was registered in SisGen under code A4E65A0.

### Extraction and crystallization

The botanical material was dried in an air circulation oven (45 °C, 24 h), and pulverized in a knife mill. The powder (2250 g) was submitted to the maceration with ethanol (99.5%, 3 × 5 L) at room temperature. The extracting liquid was then filtered and concentrated on a rotary evaporator to afford the crude ethanolic extract (189.6 g). The ethanolic extract was fractionated by vacuum filtration with the incorporation of microcrystalline cellulose D and passing of hexane, ethyl acetate, and methanol to yield the respective fractions: hexane (7.1 g), ethyl acetate (22.8 g), and methanolic (99.6 g). The hexane fraction (5 g) was fractionated on a silica gel column (4.5 × 15.0 cm) eluted with hexane/AcOEt (9:1, 8:2, 7:3, 6:4, 5:5, 3:7, 1:9, v/v), AcOEt, AcOEt/MeOH (1:1, v/v) and MeOH to yield fractions H1-H15. Fraction H5 (185 mg) was subjected to a silica gel column (2.4 × 20.0 cm) eluted with hexane/EtOAc (9:1, 8:2 v/v) to afford 27 fractions, which were pooled into 6 subfractions (H5.1-H5.6) after TLC analysis. Fraction H5.5 (75 mg) was subjected to a silica gel column (1.5 × 24.0 cm) eluted with hexane/EtOAc (8.5:1.5, v/v) to yield the STR compound (18.2 mg). The <sup>1</sup>H NMR spectrum (500 MHz, CDCl<sub>3</sub>) (Figure S1), <sup>13</sup>C NMR spectrum (125 MHz, CDCl<sub>3</sub>) (Figure S2) and infrared spectrum of  $\beta$ -sitosterol (Figure S3) are present in Supplementary Information (SI) section.

### Crystallographic characterization

Single-crystal XRD data collection was performed on a Bruker PHOTON-II diffractometer (Agilent SuperNova, Notre Dame, USA) applying a combination of  $\omega$ - and  $\phi$ -scans of 0.5°. Data were corrected for absorption and polarization effects and analyzed for space group determination.<sup>37</sup> The structure was solved by dual-space methods<sup>38</sup> and refined by full-matrix least-squares analysis of  $F^2$  against all reflections.<sup>39</sup> Anisotropic atomic displacement parameters were used to refine all non-hydrogen atoms. Atomic displacement for the hydrogens was placed to the equivalent isotropic displacement parameter ( $U_{iso}(H) = 1.5U_{eq}(C)$  for methyl,  $1.2U_{eq}(C)$  for all others) according to the riding model. The crystallographic information file (CIF) was

deposited at the Cambridge Crystallographic Data Center (CCDC) under deposit number 2182940.

### Hirshfeld surface

The HS was calculated over the crystallographic structure (obtained experimentally through XRD), without optimization of the geometric parameters. The analysis of the HS was used to visualize and interpret the potential intermolecular interactions, which can produce a 2D fingerprint histogram, by plotting the fraction of points on the surface as a function of the ( $d_i$  and  $d_e$ ) pair.<sup>40</sup> On an HS the normalized contact distance ( $d_{norm}$ ) is defined from the distance of atoms external ( $d_e$ ), and internal ( $d_i$ ) to the surface, through CrystalExplorer software,<sup>41</sup> using the van der Waals radius, described in equation 1:

$$d_{norm} = (d_i - r_i^{vdw}) / r_i^{vdw} + (d_e - r_e^{vdw}) / r_e^{vdw} \quad (1)$$

where  $r^{vdw}$  represented the van der Waals radii of the atoms.<sup>42</sup> The graphical representation of  $d_{norm}$  uses color coding system to identify intermolecular interactions, with the sum of the van der Waals radii. Different levels of color are associated with the intensity of interactions, where blue and red indicates long and short intermolecular contacts, respectively.<sup>42</sup>

### Theoretical calculation

The geometric parameters obtained experimentally through XRD were optimized in the gas phase by the Gaussian09 software,<sup>43</sup> the conformers (STR-I and STR-II) were individually optimized through density functional

theory (DFT)<sup>44</sup> applying M06-2X/6-311++G(d,p) level of theory,<sup>45-47</sup> which is suitable for non-covalent interactions.<sup>45,48</sup> From the results generated in the optimization, FMO, and the MEP were calculated for each conformer. The highest occupied molecular orbital (HOMO) and the lowest unoccupied molecular orbital (LUMO) can indicate kinetic stability and chemical reactivity of the molecule, and characterize  $\pi^*$  antibonding and nonbonding orbitals and their nucleophilic/electrophilic regions.<sup>49,50</sup> The MEP map also contributes to identifying the reactive regions of a molecule and regions of nucleophilic/electrophilic attack; to build this surface of electrostatic potential, we used a function that considers the potential created by the nucleus and electrons, as shown in equation 2:

$$V(\mathbf{r}) = \sum_A \frac{Z_A}{|\mathbf{R}_A - \mathbf{r}|} - \int \frac{\rho(\mathbf{r}')}{|\mathbf{r}' - \mathbf{r}|} d\mathbf{r}' \quad (2)$$

$V(\mathbf{r})$  is a potential created at a defined point, the first term of summation is the electrostatic potential created by the nucleus, while the second term of summation is the electrostatic potential created by electrons.<sup>51</sup>

## Results and Discussion

### Solid-state characterization

The STR was crystallized in the non-centrosymmetric monoclinic space group  $P2_1$ , with two independent molecules (STR-I and STR-II), complexed with one water molecule (Figure 1), in the asymmetric unit. The conformers differ in the aliphatic chain site, indicating a conformational polymorphism in the crystalline state.<sup>52</sup>

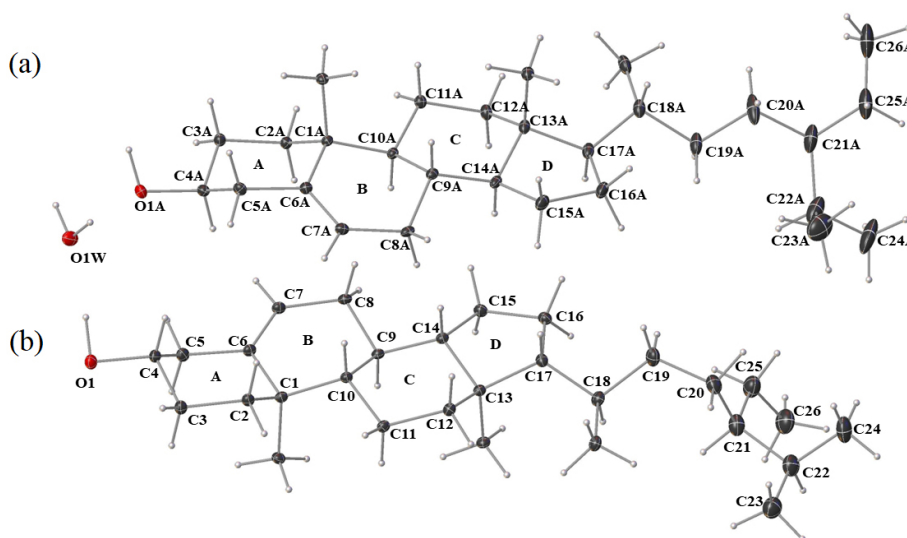


**Figure 1.** Oak Ridge Thermal Ellipsoid Plot (ORTEP) diagram of ellipsoids at 30% probability level with the atomic numbering scheme for (a) STR-I, and (b) STR-II.

Each conformer has nine chiral carbons (C1, C13, C17, C18 and C21 in *R* conformation; C4, C9, C10 and C14 in *S* conformation). Their crystallographic parameters and refinement data are shown in Table 1.

**Table 1.** Crystal data and structure refinement for STR

Empirical formula	$C_{58}H_{102}O_3$	
Formula weight / (g mol <sup>-1</sup> )	847.39	
Temperature / K	120(2)	
Crystal system	monoclinic	
Space group	$P2_1$	
Unit cell dimensions	$a = 9.4367(3) \text{ \AA}$	$\alpha = 90^\circ$
	$b = 7.4860(3) \text{ \AA}$	$\beta = 93.250(2)^\circ$
	$c = 36.9087(13) \text{ \AA}$	$\gamma = 90^\circ$
Volume / $\text{\AA}^3$	2603.15(16)	
Z	2	
Absorption coefficient / ( $\mu \text{ mm}^{-1}$ )	0.476	
F(000)	948	
$\theta$ range for data collection / degree	2.398 to 70.750	
Index ranges	$-11 \leq h \leq 11, -8 \leq k \leq 8, -44 \leq l \leq 44$	
Reflections collected	54528	
Independent reflections	9775 [ $R_{\text{int}} = 0.0629$ ]	
Absorption correction	numerical	
Max. and min. transmission	0.9849 and 0.8766	
Goodness-of-fit on $F^2$	1.026	
Final $R$ indices [ $I > 2\sigma(I)$ ]	$R_1 = 0.0752, wR_2 = 0.2002$	
$R$ indices (all data)	$R_1 = 0.0921, wR_2 = 0.2247$	
Absolute structure parameter	0.04(13)	
Largest diff. peak and hole / ( $e \text{ \AA}^{-3}$ )	0.633 and $-0.383$	

Z: formula unit *per* unit cell;  $R_1$ :  $R$ -value;  $wR_2$ :  $R$ -value for  $F^2$ .

The STR compound has three rings with six members and one ring with five members. Rings A and C have a chair conformation, while ring B has a half-chair conformation. The overlap of STR-I and STR-II demonstrates the value of the root mean square (RMS) = 0.0363, which measures the geometric difference in the structures. These differences can be evidenced by the dihedral angles of atoms C18A–C19A–C20A–C21A ( $-170.3(9)^\circ$ ) and C18–C19–C20–C21 ( $63.9(9)^\circ$ ), not overlapping the ethyl radicals and the isopropyl radicals (Figure 2).

The supramolecular arrangement is formed by  $O1W-H1WA \cdots O1A$ ,  $O1W-H1WB \cdots O1A$ ,  $O1-H1 \cdots O1W$  and  $O1A-H1A \cdots O1$  interactions (Table 2), appearing as a ring coordinated by two water molecules related by a twofold screw axis along the  $b$  axis, which can be described as  $R_2^2(10)$ , as shown in Figure 3a. Also, Figure 3b shows the crystal packing of STR, which is formed by a three-

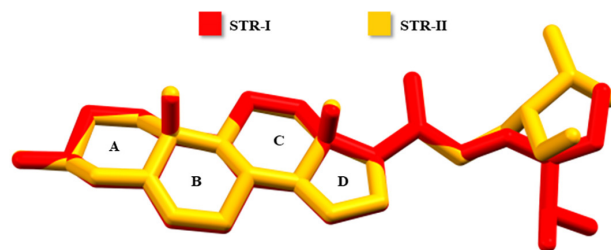


**Figure 2.** Overlap of STR-I and STR-II. Hydrogen atoms were omitted.

dimensional network described as a “chain of rings” lying at the center of the unit cell. To compare the structure of STR with other water-complexed sterols, mainly concerning the supramolecular arrangement, similar structures were selected from the CCDC: stigmast-5-en-3-ol hemihydrate (code 1434206-STS I<sup>53</sup> and code 1985852-STS II).<sup>54</sup> It is observed that both compounds exhibit the three-dimensional network which is coordinated by the water molecules, forming the “chain of rings” that can be described as  $R_2^2(10)$ . On the other hand, sterols without the water molecules, such as stigmasta-4,25-diene-3 $\beta$ ,6 $\beta$ -diol,<sup>55</sup> cholest-5-en-3-ol<sup>56</sup> and 10,13-dimethyl-17-(5-(2-methylcyclopropyl)hexan-2-yl)-2,3,4,7,8,9,10,11,12,13,14,15,16,17-tetradecahydro-1*H*-cyclopenta[*a*]phenanthren-3-ol<sup>57</sup> (code 639110, 1944206 and 1417552, respectively), exhibit only a two-dimensional crystalline packing network.

Intermolecular interactions were analyzed by the HS denominated  $d_{\text{norm}}$ , where high values of distances  $d_i$  and  $d_e$  indicate donor and acceptor regions of intermolecular contacts, represented by  $d$  and  $r$ , respectively. Color scales are used to indicate intensities of contacts, where the blue color represents weaker contacts and the red color represents stronger contacts. In Figure 4a, the molecule inside the surface is STR-I; the red dots (1r) and (2r) correspond to  $d_e$  contacts indicating that they act as acceptors for  $O1W-H1WB \cdots O1A$  and  $O1W-H1WA \cdots O1A$ , respectively. In Figure 4b, the molecule inside the surface is STR-II; the red dot (3d) corresponds to  $d_i$  contacts, indicating where the molecule acts as a donor of  $O1-H1 \cdots O1W$ , and the red dot (4r) corresponds to  $d_e$  contacts, indicating where the molecule acts as an acceptor of  $O1A-H1A \cdots O1$ .

The combination of  $d_e$  and  $d_i$  distance functions provides a mapping of all contacts present in the molecule, and their percentage contribution to each type of interaction present, making the fingerprints unique for each compound. Figure 5 represents the fingerprint of the STR interactions, where the  $H \cdots H$  weak contacts (region  $d_e = d_i = 1.2 \text{ \AA}$ ) represent the majority of all observed contacts making up 93.7% of the HS. The  $O \cdots H$  contacts constitute the second-largest percentage in the STR compound making up 5.4% of the total surface, and were detected as a spike

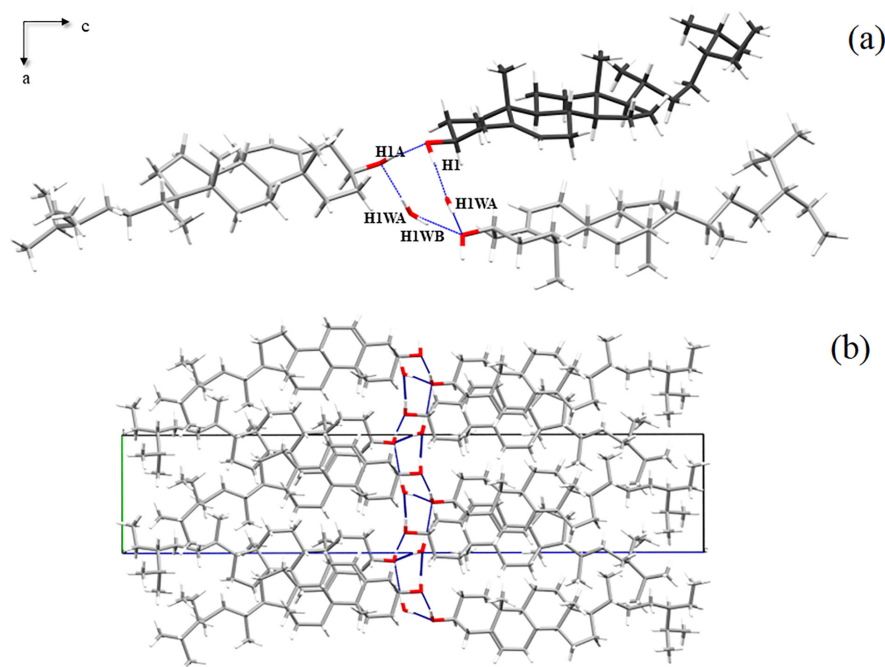


**Figure 3.** Representation of (a) supramolecular arrangement, where the STR-I is represented by gray, and STR-II by black, showing the ring formed by interactions O1W–H1WA–O1A, O1W–H1WB–O1A, O1–H1–O1W and O1A–H1A–O1 and (b) the crystalline packing of STR.

**Table 2.** Hydrogen bond distances and angles for STR

D–H···A	D–H / Å	H···A / Å	D···A / Å	D–H···A / degree	Symmetry code
O1W–H1WB···O1A	0.99	2.25	3.224	169	$-x, -1/2+y, 1-z$
O1W–H1WA···O1A	0.81	2.00	2.813	174	$x, y, z$
O1–H1–O1W	1.02	1.86	2.877	174	$x, -1+y, z$
O1A–H1A–O1	0.99	1.79	2.762	168	$-x, -1/2+y, 1-z$

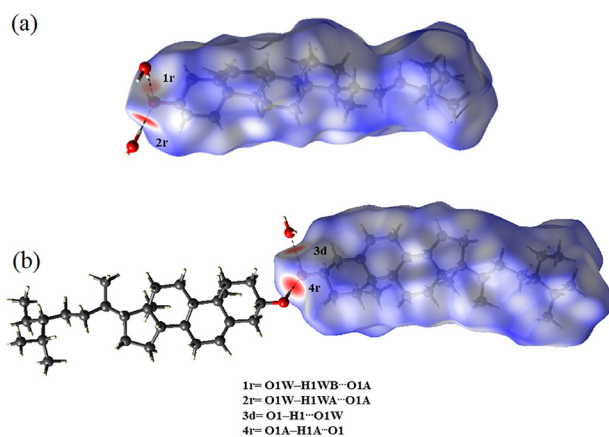


**Figure 4.** Hirshfeld surface  $d_{norm}$  mapped indicating intermolecular interactions of STR-I (a), and STR-II (b). The dotted black lines represent hydrogen bonds.

with  $d_e = 1.1 \text{ \AA}$  and  $d_i = 0.7 \text{ \AA}$ . The H···C interactions represent 0.8% of the total surface in the top region of the fingerprint plot with no important role in the stabilization of the structure. The compound does not have stabilized packing by  $\pi \cdots \pi$  interactions.

### Molecular modeling

The RMS values, predicted by Mercury software,<sup>58</sup> between conformers (STR-I and STR-II) experimental geometries and theoretical calculation were 0.0179 and 0.0096, respectively. The overlappings of the M062X/6-311+G(d,p) level of theory (yellow) and X-ray (black) for conformers (STR-I and STR-II) are shown in Figures 6a and 6b, respectively. The comparative graphs (experimental geometries and theoretical calculation) for the bond lengths and angles obtained for STR-I and STR-II are shown in Figure 7. The mean absolute percentage deviations (MAPD) were defined by equation 3:

$$\text{MAPD} = \frac{100}{n} \sum_{i=1}^n \left| \frac{\chi_{XRD} - \chi_{DFT}}{\chi_{XRD}} \right| \quad (3)$$

where  $\chi_{XRD}$  and  $\chi_{DFT}$  represents the geometric parameters for the theoretical calculation and experimental geometrical data, respectively. The MAPD values for STR-I bond lengths and angles were 0.720 and 0.509, respectively. The Pearson

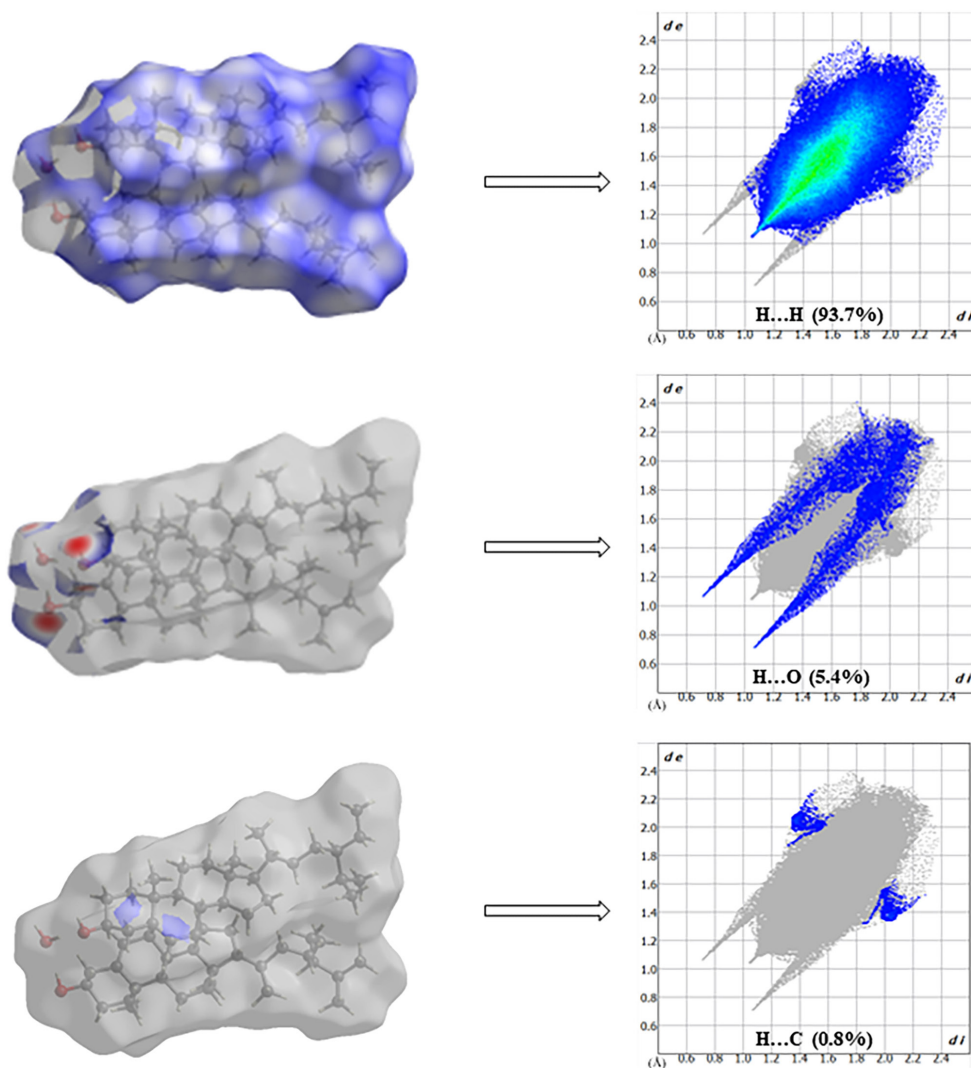


**Figure 5.** Fingerprint and quantification of different types of contacts of STR.

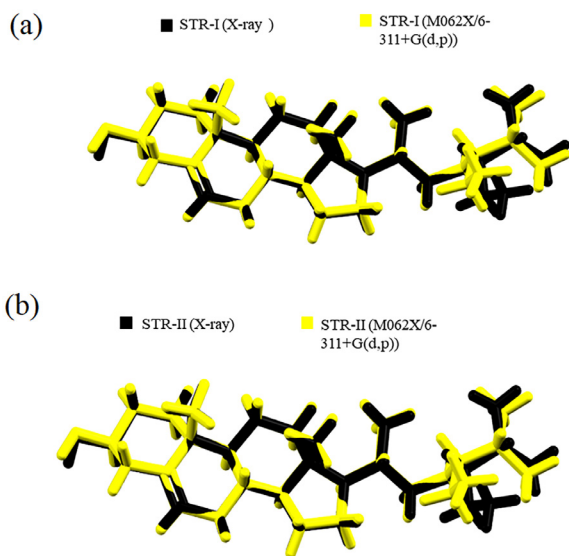


**Figure 6.** Overlapping between the experimental X-ray data (black) and the M062X/6-311+G(d,p) level of theory (yellow) structures for (a) STR-I and (b) STR-II.

correlation coefficient ( $R^2$ ) values were 0.8975 and 0.9846 for experimental geometries and theoretical calculation data for STR-I. For STR-II, the MAPD values bond lengths and angles were 0.659 and 0.648, respectively. The  $R^2$  values for STR-II experimental geometries and theoretical calculation data were 0.9429 and 0.9773, respectively.

The calculated HOMO orbital for STR conformers was located on rings A and B (both in STR-I and STR-II), while the LUMO orbital was also similar for both (STR-I and STR-II) and was spread in the molecule (Figure 8). The LUMO energy was  $-20.47 \text{ kJ mol}^{-1}$  for STR-I and  $-19.87 \text{ kJ mol}^{-1}$  for STR-II, and this orbital characterizes  $\pi^*$  antibonding, with negative energy indicating electrophilic regions, susceptible to accept electrons in a chemical reaction. The energy difference between these orbitals ( $E_{\text{GAP}} = E_{\text{LUMO}} - E_{\text{HOMO}}$ ) is an important indicator of the kinetic stability and chemical reactivity of the molecule,<sup>49</sup> because it is energetically unfavorable to add electrons to a high-lying LUMO and to

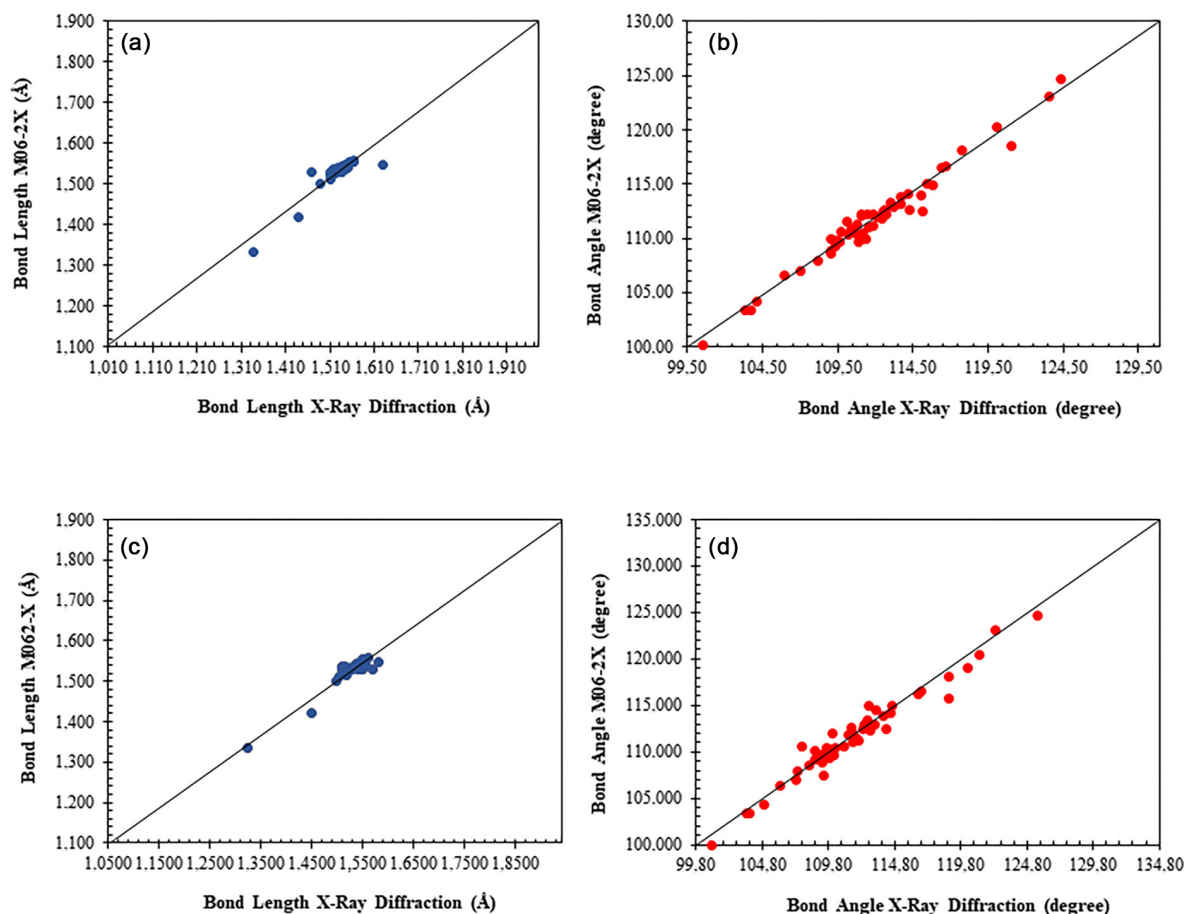


**Figure 7.** The comparative graphs of the geometric (a) bond length and (b) angle for STR-I, and (c) bond length and (d) angle for STR-II, obtained by experimental X-ray and theoretical calculation data.

extract electrons from a low-lying HOMO, and so to form the activated complex of any potential reaction.<sup>59</sup> The  $E_{\text{GAP}}$  is  $738.92 \text{ kJ mol}^{-1}$  for STR-I and  $740.08 \text{ kJ mol}^{-1}$  for STR-II, respectively.

The MEP map calculated for the STR compound is related to the local charges. The red colors indicate regions susceptible to electrophilic attack and are on the O1A

(STR-I) and O1 (STR-II) atoms, while blue colors are susceptible to nucleophilic attacks,<sup>51,60,61</sup> they are on the H1A (STR-I) and H1 (STR-II) atoms. It should be noted that these regions correspond to the O1W–H1WB··O1A, O1W–H1WA··O1A, O1–H1··O1W and O1A–H1A··O1 interactions, which have been described by geometrical parameters and electronic density. Figure 9 shows the MEP map surfaces with isovalues of  $\pm 0.0004$ .

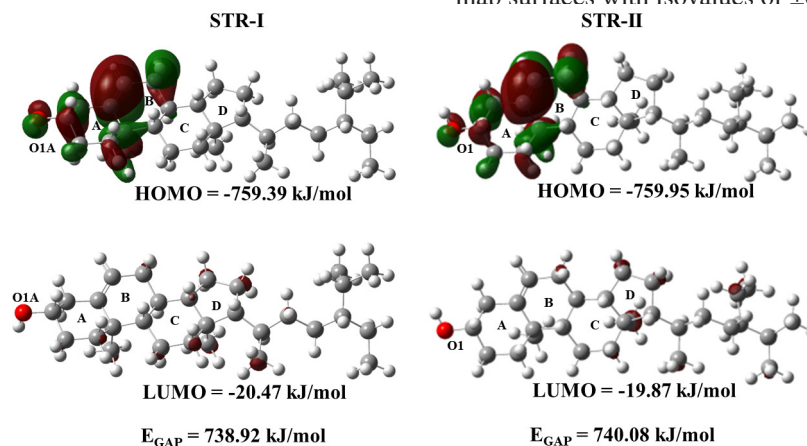


**Figure 8.** Molecular orbitals HOMO/LUMO for STR conformers (isovalues  $\pm 0.02 \text{ au}$ ).

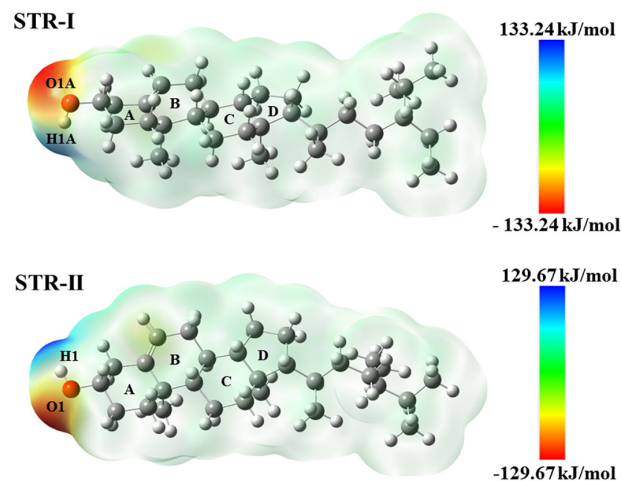


Figure 9. MEP map for STR compound (isovalues  $\pm 0.0004$  au).

### Vibrational assignments

The main IR absorption bands are in Table 3 and the theoretical and experimental FTIR spectra for STR-I and STR-II conformers are in Figure 10. The values in vibrational frequencies obtained at M06-2X/6-311++G(d,p) level of theory were scaled by Yin and Kong<sup>62</sup> as 0.943. Theoretical measurements of  $\nu(\text{O-H})$  for STR-I and STR-II conformers, obtained in the gas phase, absorb at 3687  $\text{cm}^{-1}$ , while the experimental measurements occur at 3424  $\text{cm}^{-1}$ . This decrease of the experimental vibrational frequency value for  $\nu(\text{O-H})$  occurs due to the molecular hydrogen interactions. Absorption peaks appear in the experimental  $\nu(\text{C=C})$  for STR-I and STR-II conformers at 1651  $\text{cm}^{-1}$ , while the theoretical measurements absorb at 1658  $\text{cm}^{-1}$ . The  $\nu(\text{C}_{\text{sp}}^3\text{-H})$  for STR-I and STR-II conformers is in the range of 2936–2861  $\text{cm}^{-1}$ , while the DFT calculations assigned at the region of 2936–2877  $\text{cm}^{-1}$ .

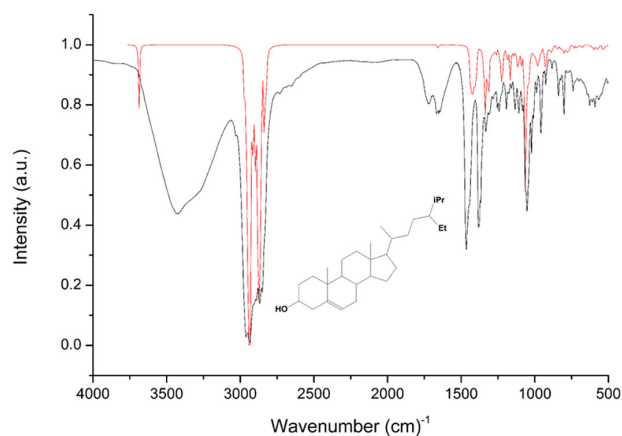


Figure 10. Overlapping of the theoretical (red) and experimental (black) FTIR (KBr) spectra of STR-I and STR-II conformers.

Table 3. Vibrational assignments of the theoretical and experimental FTIR for STR-I and STR-II conformers. These results were obtained at M06-2X/6-311++G(d,p) level of theory in the gas phase

Vibrational mode	STR-I and STR-II conformers	
	Experimental frequency / $\text{cm}^{-1}$	Scaled frequency <sup>a</sup> / $\text{cm}^{-1}$
$\nu(\text{O-H})$	3424	3687
$\nu(\text{C}_{\text{sp}}^3\text{-H})$	2936-2861	2936-2877
$\nu(\text{C=C})$	1651	1658
$\delta(\text{CH}_2)_n \text{Cyc}^a$	1466	1426
$\delta(\text{CH}(\text{CH}_3)_2)_{\text{Gem}}^b$	1377	1333
$\nu(\text{C-O})$	1053	1063

<sup>a</sup>Cyclic methylene groups; <sup>b</sup>gem-dimethyl group.  $\nu$ : stretching;  $\delta$ : bending.

### Conclusions

The  $\beta$ -sitosterol compound was crystallized with two independent conformers and one water molecule in the asymmetric unit. The title compound was overlaid, and differences were evidenced from the dihedral angles of carbons C18–C19–C20–C21, not overlapping the ethyl radicals and the isopropyl radicals. The supramolecular arrangement was stabilized by classical hydrogen O–H···O bonding, forming a ‘chain of rings’, which is also observed in similar compounds researched at CCDC. The kinetic stability of the compound was confirmed through the high value found (738.92  $\text{kJ mol}^{-1}$  for STR-I and 740.08  $\text{kJ mol}^{-1}$  for STR-II). The MEP analysis reveals that the oxygen region is susceptible to electrophilic attack. The structural study of a sterol extracted from the Brazilian Cerrado offers a new and deeper understanding of the biodiversity of sterols.

### Supplementary Information

Crystallographic data (excluding structure factors) for the structures in this work were deposited in the Cambridge Crystallographic Data Centre as supplementary publication number CCDC 2182940. Copies of the data can be obtained, free of charge, via <https://www.ccdc.cam.ac.uk/structures/>.

The supplementary information contains figures of infrared and NMR spectroscopies, and it is available free of charge at <http://jbcs.sbc.org.br> as a PDF file.

### Acknowledgments

The authors are grateful to the Conselho Nacional de Desenvolvimento Científico e Tecnológico (CNPq), the Fundação Nacional de Desenvolvimento do Ensino

Superior Particular (FUNADESP) and the Fundação de Amparo a Pesquisa do Estado de Goiás (FAPEG) for financial support. They thank Prof Dr Mirley Luciene dos Santos for identifying the species collected, and the University of Notre Dame for X-ray collection of STR. The authors are also grateful to the High-Performance Computing Center of the Universidade Estadual de Goiás (UEG), which was used for performing theoretical calculations.

### Author Contributions

Marianna C. Silva was responsible for the introduction, crystallographic characterization, results, discussion, writing the original draft, review, and editing; Vitor S. Duarte and Lóide O. Sallum were responsible for computational methodology, results, discussion, and review; Gracielle O. S. Cunha and Antônio C. S. Menezes for extraction, crystallization, infrared and NMR spectroscopies; Josana C. Peixoto for the botanical studies; Jean M. F. Custodio and Allen G. Oliver for X-ray collection and review; Hamilton B. Napolitano was responsible for conceptualization, crystallographic characterization, review and supervision.

### References

1. Strassburg, B. B. N.; Brooks, T.; Feltran-Barbieri, R.; Iribarrem, A.; Crouzeilles, R.; Loyola, R.; Latawiec, A. E.; Oliveira Filho, F. J. B.; Scaramuzza, C. A. M.; Scarano, F. R.; Soares-Filho, B.; Balmford, A.; *Nat. Ecol. Evol.* **2017**, *1*, 0099. [Crossref]
2. Del-Claro, K.; Torezan-Silingardi, H. M.; *An. Acad. Bras. Cienc.* **2019**, *91*, e20180768. [Crossref]
3. Ribeiro Neto, J. A.; Tarôco, B. R. P.; dos Santos, H. B.; Thomé, R. G.; Wolfram, E.; Ribeiro, R. I. M. A.; *J. Ethnopharmacol.* **2020**, *260*, 112547. [Crossref]
4. Colli, G. R.; Vieira, C. R.; Dianese, J. C.; *Biodiversity Conserv.* **2020**, *29*, 1465. [Crossref]
5. Carneiro, M. R. B.; Sallum, L. O.; Martins, J. L. R.; Peixoto, J. C.; Napolitano, H. B.; Rosseto, L. P.; *Molecules* **2023**, *28*, 1190. [Crossref]
6. Fank-de-Carvalho, S. M.; Somavilla, N. S.; Marchioretto, M. S.; Bão, S. N. In *Biodiversity in Ecosystems*, vol. 1; Lo, Y.-H.; Blanco, J. A.; Roy, S., eds.; InTech: London, UK, 2015.
7. Bailão, E. F. L. C.; Devilla, I. A.; da Conceição, E. C.; Borges, L. L.; *Int. J. Mol. Sci.* **2015**, *16*, 23760. [Crossref]
8. Rosa, M. N.; e Silva, L. R. V.; Longato, G. B.; Evangelista, A. F.; Gomes, I. N. F.; Alves, A. L. v.; de Oliveira, B. G.; Pinto, F. E.; Romão, W.; de Rezende, A. R.; Araújo, A. A. C.; Oliveira, L. S. F. M.; Souza, A. A. M.; Oliveira, S. C.; Ribeiro, R. I. M. A.; Silva, V. A. O.; Reis, R. M.; *Int. J. Mol. Sci.* **2021**, *22*, 3383. [Crossref]
9. de Carvalho, J. T. G.; Baldivia, D. S.; Leite, D. F.; de Araújo, L. C. A.; Espindola, P. P. T.; Antunes, K. A.; Rocha, P. S.; Souza, K. P.; dos Santos, E. L.; *Oxid. Med. Cell. Longevity* **2019**, *2019*, ID 3685264. [Crossref]
10. Valli, M.; Russo, H. M.; Bolzani, V. S.; *An. Acad. Bras. Cienc.* **2018**, *90*, 763. [Crossref]
11. Sabbag Cunha, G. O.; da Cruz, D. C.; Severo Menezes, A. C.; *Pharmacogn. Rev.* **2021**, *13*, 77. [Crossref]
12. Torres, L. R. O.; Shinagawa, F. B.; Santana, F. C.; Araújo, E. S.; Oropeza, M. V. C.; Macedo, L. F. L.; Almeida-Muradian, L. B.; Lima, H. C.; Mancini-Filho, J.; *Int. Food. Res. J.* **2016**, *23*, 1541. [Crossref]
13. da Costa, P. A.; Ballus, C. A.; Teixeira-Filho, J.; Godoy, H. T.; *Food Res. Int.* **2010**, *43*, 1603. [Crossref]
14. Ayres, M. C. C.; Escórcio, S. P.; da Costa, D. A.; Chaves, M. H.; Vieira Jr., G. M.; Cavalheiro, A. J.; *Quim. Nova* **2008**, *31*, 1481. [Crossref]
15. Mota, G. S.; Sartori, C. J.; Ferreira, J.; Miranda, I.; Quilhó, T.; Mori, F. A.; Pereira, H.; *Ind. Crops Prod.* **2016**, *90*, 65. [Crossref]
16. de Bessa, N. G. F.; Borges, J. C. M.; Beserra, F. P.; Carvalho, R. H. A.; Pereira, M. A. B.; Fagundes, R.; Campos, S. L.; Ribeiro, L. U.; Quirino, M. S.; Chagas Jr., A. F.; Alves, A.; *Rev. Bras. Plantas Med.* **2013**, *15*, 692. [Crossref]
17. Sherwin, E. R.; *J. Am. Oil Chem. Soc.* **1978**, *55*, 809. [Crossref]
18. Barbas, R.; Bofill, L.; de Sande, D.; Font-Bardia, M.; Prohens, R.; *CrystEngComm* **2020**, *22*, 4210. [Crossref]
19. Moreno-Calvo, E.; Temelli, F.; Cordoba, A.; Masciocchi, N.; Veciana, J.; Ventosa, N.; *Cryst. Growth Des.* **2014**, *14*, 58. [Crossref]
20. Weihrauch, J. L.; Gardner, J. M.; *J. Am. Diet. Assoc.* **1978**, *73*, 39. [Crossref]
21. Radika, M. K.; Viswanathan, P.; Anuradha, C. V.; *Nitric Oxide* **2013**, *32*, 43. [Crossref]
22. de Lima, R. C.; Mendonça, V. S.; Huguenin, G. V. B.; *Braz. J. Health Rev.* **2021**, *4*, 16317. [Crossref]
23. Nirmal, S. A.; Pal, S. C.; Mandal, S. C.; Patil, A. N.; *Inflammopharmacology* **2012**, *20*, 219. [Crossref]
24. Subramaniam, S.; Keerthiraja, M.; Sivasubramanian, A.; *Rev. Bras. Farmacogn.* **2014**, *24*, 44. [Crossref]
25. Kiprono, P. C.; Kaberia, F.; Keriko, J. M.; Karanja, J. N.; *Z. Naturforsch., C: J. Biosci.* **2000**, *55*, 485. [Crossref]
26. Sharmila, R.; Sindhu, G.; *Pharmacogn. Mag.* **2017**, *13*, 95. [Crossref]
27. Awad, A. B.; Roy, R.; Fink, C. S.; *Oncol. Rep.* **2003**, *10*, 497. [Crossref]
28. Muti, P.; Awad, A. B.; Schünemann, H.; Fink, C. S.; Hovey, K.; Freudenheim, J. L.; Wu, Y.-W. B.; Bellati, C.; Pala, V.; Berrino, F.; *J. Nutr.* **2003**, *133*, 4252. [Crossref]
29. Paniagua-Pérez, R.; Flores-Mondragón, G.; Reyes-Legorreta, C.; Herrera-López, B.; Cervantes-Hernández, I.; Madrigal-

- Santillán, O.; Morales-González, J. A.; Álvarez-González, I.; Madrigal-Bujaidar, E.; *Afr. J. Tradit., Complementary Altern. Med.* **2016**, *14*, 123. [Crossref]
30. Park, Y. J.; Bang, I. J.; Jeong, M. H.; Kim, H. R.; Lee, D. E.; Kwak, J. H.; Chung, K. H.; *J. Agric. Food Chem.* **2019**, *67*, 9789. [Crossref]
31. Abdou, E. M.; Fayed, M. A. A.; Helal, D.; Ahmed, K. A.; *Sci. Rep.* **2019**, *9*, 19779. [Crossref]
32. Ponnulakshmi, R.; Shyamaladevi, B.; Vijayalakshmi, P.; Selvaraj, J.; *Toxicol. Mech. Methods* **2019**, *29*, 276. [Crossref]
33. Abbas, M.; Al-Rawi, N.; Abbas, M.; Al-Khateeb, I.; *Res. Pharm. Sci.* **2019**, *14*, 566. [Crossref]
34. Babu, S.; Krishnan, M.; Rajagopal, P.; Periyasamy, V.; Veeraraghavan, V.; Govindan, R.; Jayaraman, S.; *Eur. J. Pharmacol.* **2020**, 873, 173004. [Crossref]
35. Babu, S.; Jayaraman, S.; *Biomed. Pharmacother.* **2020**, *131*, 110702. [Crossref]
36. APEX3, SAINT and SADABS; Bruker AXS Inc., Madison, USA, 2016.
37. Krause, L.; Herbst-Irmer, R.; Sheldrick, G. M.; Stalke, D.; *J. Appl. Crystallogr.* **2015**, *48*, 3. [Crossref]
38. Sheldrick, G. M.; *Acta Crystallogr., Sect. A: Found. Adv.* **2015**, *A71*, 3. [Crossref]
39. Sheldrick, G. M.; *Acta Crystallogr., Sect. C: Struct. Chem.* **2015**, *C71*, 3. [Crossref]
40. Spackman, M. A.; Mckinnon, J. J.; *CrystEngComm* **2002**, *4*, 378. [Crossref]
41. Wolff, S. K.; Grimwood, D. J.; McKinnon, J. J.; Turner, M. J.; Jayatilaka, D.; Spackman, M. A.; *Crystal Explorer*, v. 3.0, University of Western/Perth, Australia, 2012.
42. Spackman, M. A.; Jayatilaka, D.; *CrystEngComm* **2009**, *11*, 19. [Crossref]
43. Frisch, M. J.; Trucks, G. W.; Schlegel, H. B.; Scuseria, G. E.; Robb, M. A.; Cheeseman, J. R.; Scalmani, G.; Barone, V.; Mennucci, B.; Petersson, G. A.; Nakatsuji, H.; Caricato, M.; Li, X.; Hratchian, H. P.; Izmaylov, A. F.; Bloino, J.; Zheng, G.; Sonnenberg, J. L.; Hada, M.; Ehara, M.; Toyota, K.; Fukuda, R.; Hasegawa, J.; Ishida, M.; Nakajima, T.; Honda, Y.; Kitao, O.; Nakai, H.; Vreven, T.; Montgomery, Jr., J. A.; Peralta, J. E.; Ogliaro, F.; Bearpark, M.; Heyd, J. J.; Brothers, E.; Kudin, K. N.; Staroverov, V. N.; Kobayashi, R.; Normand, J.; Raghavachari, K.; Rendell, A.; Burant, J. C.; Iyengar, S. S.; Tomasi, J.; Cossi, M.; Rega, N.; Millam, J. M.; Klene, M.; Knox, J. E.; Cross, J. B.; Bakken, V.; Adamo, C.; Jaramillo, J.; Gomperts, R.; Stratmann, R. E.; Yazyev, O.; Austin, A. J.; Cammi, R.; Pomelli, C.; Ochterski, J. W.; Martin, R. L.; Morokuma, K.; Zakrzewski, V. G.; Voth, G. A.; Salvador, P.; Dannenberg, J. J.; Dapprich, S.; Daniels, A. D.; Farkas, Ö.; Foresman, J. B.; Ortiz, J. V.; Cioslowski, J.; Fox, D. J.; *Gaussian 09, Revision A.02*, Gaussian Inc., Wallingford CT, 2009.
44. Burke, K.; *J. Chem. Phys.* **2012**, *136*, 150901. [Crossref]
45. Zhao, Y.; Truhlar, D. G.; *Theor. Chem. Acc.* **2008**, *120*, 215. [Crossref]
46. Krishnan, R.; Binkley, J. S.; Seeger, R.; Pople, J. A.; *J. Chem. Phys.* **1980**, *72*, 650. [Crossref]
47. McLean, A. D.; Chandler, G. S.; *J. Chem. Phys.* **1980**, *72*, 5639. [Crossref]
48. Hohenstein, E. G.; Chill, S. T.; Sherrill, C. D.; *J. Chem. Theory. Comput.* **2008**, *4*, 1996. [Crossref]
49. Pereira, D. H.; la Porta, F. A.; Santiago, R. T.; Garcia, D. R.; Ramalho, T. C.; *Rev. Virtual Quim.* **2016**, *8*, 425. [Crossref]
50. Houk, K. N.; *Nature* **1977**, *266*, 662. [Crossref]
51. Sjöberg, P.; Politzer, P.; *J. Phys. Chem.* **1990**, *94*, 3959. [Crossref]
52. Ikonen, S.; Jurček, O.; Wimmer, Z.; Drašar, P.; Kolehmainen, E.; *J. Mol. Struct.* **2012**, *1011*, 25. [Crossref]
53. Guercia, E.; Berti, F.; Navarini, L.; Demitri, N.; Forzato, C.; *Tetrahedron: Asymmetry* **2016**, *27*, 649. [Crossref]
54. Yang, Y.; Yong, J.-P.; Olagoke, Z. O.; Lu, C.-Z.; Huaxue, J.; *Chin. J. Struct. Chem.* **2021**, *40*, 653. [Crossref]
55. He, Z.-Z.; Lei, X.-X.; Zhou, Y.; Sun, J.-Z.; Zhang, A.-J.; *Z. Kristallogr. - New Cryst. Struct.* **2006**, *221*, 477. [Crossref]
56. Tyler, A. R.; Ragbirsingh, R.; McMonagle, C. J.; Waddell, P. G.; Heaps, S. E.; Steed, J. W.; Thaw, P.; Hall, M. J.; Probert, M. R.; *Chem* **2020**, *6*, 1755. [Crossref]
57. Cheng, Z.; Liu, D.; de Voogd, N. J.; Proksch, P.; Lin, W.; *Helv. Chim. Acta* **2016**, *99*, 588. [Crossref]
58. Allen, F. H.; *Mercury*, v. 4.0; Cambridge Crystallographic Data Centre/Boston, United States, 2020.
59. Manolopoulos, D. E.; May, J. C.; Down, S. E.; *Chem. Phys. Lett.* **1991**, *181*, 105. [Crossref]
60. Politzer, P.; Laurence, P. R.; Jayasuriya, K.; *Environ. Health. Perspect.* **1985**, *61*, 191. [Crossref]
61. Murray, J. S.; Politzer, P.; *WIREs Comput. Mol. Sci.* **2011**, *1*, 153. [Crossref]
62. Yin, H.; Kong, X.; *J. Am. Soc. Mass Spectrom.* **2015**, *26*, 1455. [Crossref]

Submitted: July 27, 2022

Published online: March 20, 2023

